




Microstructural and electrical investigation of flash-sintered Gd/Sm-doped ceria

L. Spiridigliozzi¹, M. Biesuz², G. Dell'Agli^{1,4,*} , E. Di Bartolomeo^{3,4}, F. Zurlo³, and V. M. Sglavo^{2,4}

¹Department of Civil and Mechanical Engineering, University of Cassino and Southern Lazio, Via G. Di Biasio 43, 03043 Cassino, FR, Italy

²Department of Industrial Engineering, University of Trento, Via Sommarive 9, 38123 Trento, Italy

³Department of Chemical Sciences and Technology, University of Roma Tor Vergata, Rome, Italy

⁴National Interuniversity Consortium of Materials Science and Technology (INSTM), Via G. Giusti 9, 50121 Florence, Italy

Received: 16 December 2016

Accepted: 6 March 2017

Published online:
16 March 2017

© Springer Science+Business
Media New York 2017

ABSTRACT

Ceria-based ceramics can be considered among the most promising solid electrolytes for intermediate-temperature solid oxide fuel cells (IT-SOFC). In the present work, variously doped nanocrystalline ceria powders were flash-sintered, and the role of doping (Gd and Sm, 5–20 mol%) and sintering aid (Li and Co) on the final microstructure and the electrical behavior was investigated. Gd- or Sm-doped nanocrystalline ceria powders were synthesized by co-precipitation method using ammonia solution as precipitating agent. The synthesized nanopowders were characterized by DSC-TG, XRD, and nitrogen physisorption analysis. The nanopowders were isostatically pressed and flash-sintered. The relative density was measured by hydrostatic balance, and the corresponding microstructure was observed by SEM. The electrical behavior was studied by EIS. Flash-sintered powder pellets showed different behaviors depending on the dopant and sintering aid. The electrical conductivity of the samples increased by increasing the relative density. Fully dense Gd-doped ceria samples, synthesized by co-precipitation, were obtained by flash sintering in very short times at 700 °C. The total conductivity was comparable to that measured on samples sintered with conventional route at much higher temperatures such as 1500 °C.

Introduction

Materials with fluorite structure AB_2 , such as ceria (CeO_2), have been extensively investigated for many environmental-friendly applications such as solid oxide fuel cells (SOFC), hydrolyzers for hydrogen

production, oxygen sensors, and ultraviolet absorbers [1–5].

The conductivity and chemical reactivity are governed by the A^{4+} site substitutions. If cerium is replaced by a lower valence rare-earth cation (Re^{3+}), oxygen vacancy concentration increases and,

Address correspondence to E-mail: dellagli@unicas.it

consequently, ionic conductivity becomes larger, according to the reaction (using Kroger–Vink notation [6]):



where Re'_{Ce} is the rare-earth cation (Re^{3+}) substituting for cation Ce^{4+} , O_O^\times is the lattice oxygen anion, and $\text{V}_\text{O}^\bullet$ is the oxygen vacancy.

Among lanthanides, Gd and Sm are the dopants inducing the largest ionic conductivity with limited activation energy because their ionic radius, i.e., Gd^{3+} (0.105 nm) or Sm^{3+} (0.108 nm), is very similar to one of the host cations, Ce^{4+} (0.097 nm) [7–9]. For this reason, very recently the authors have carried out several works about the synthesis, the sintering, and the electrical characterization of Gd- and Sm-doped ceria [10–13].

Usually, the ionic conductivity of ceramics depends also on their microstructure, strongly related to processing. For example, a densified material without any interconnected porosity is fundamental as electrolyte for SOFC applications. Unfortunately, fully dense ceria-based ceramics are very challenging because of the high firing temperatures and long required thermal treatments [14]. Several previous works reported about the sintering of ceria-based materials; as an example, Van Herle [15] pointed out that 95% relative density for yttrium-doped ceria is typically obtained at 1500–1600 °C. Using more reactive powders, sintering temperature can be reduced down to 1200–1300 °C, although long treatments remain necessary: For example, very recently, Dong [16] sintered GDC10 at 1250 °C by an 8-h thermal treatment. Moreover, sintering and densification behavior of ceria-based ceramics strongly rely on raw powder properties (e.g., particle size and particle-size distribution) [17]. An innovative technique named flash sintering (FS) has been recently established as a very promising method to get fully dense ceramics at low temperature in a very short time under the effect of an external electrical field. FS has been successfully used for a large number of ceramic materials, including also the most typical materials as electrolytes for SOFC, such as zirconia-based and ceria-based ceramics [18–22].

In the present work, FS was employed to sinter Gd- and Sm-doped ceria powders, synthesized by a co-precipitation route. The effect of the dopant concentration (5–20 mol%) and of the addition of sintering

aids (Li and Co) on sintering behavior, microstructure, and electrical behavior was investigated.

Materials and methods

Cerium (III) nitrate [$\text{Ce}(\text{NO}_3)_3 \cdot 6\text{H}_2\text{O}$ 99.0% Carlo Erba, Italy], gadolinium nitrate [$\text{Gd}(\text{NO}_3)_3 \cdot 6\text{H}_2\text{O}$ 99.0% Carlo Erba, Italy], and samarium nitrate [$\text{Sm}(\text{NO}_3)_3 \cdot 6\text{H}_2\text{O}$ 99.0% Carlo Erba, Italy] were used as raw materials for the synthesis of hydrous gadolinium-doped cerium oxides and hydrous samarium-doped cerium oxide by co-precipitation. The gadolinium content was varied between 5 and 20 mol%; thus, the reference composition of the various samples in the anhydrous form was $\text{Ce}_{1-x}\text{Gd}_x\text{O}_{2-x/2}$ with $x = 0, 0.05, 0.10, 0.15,$ and 0.20 . The samples were named C, GDC5, GDC10, GDC15, and GDC20, accordingly. The reference composition $\text{Ce}_{0.9}\text{Sm}_{0.1}\text{O}_{1.95}$ (labelled as SDC10) was obtained by using 10 mol% of samarium. The proper nitrate amount was dissolved in deionized water to get a total cationic concentration equal to 0.1 M. Then, the solution was vigorously stirred for 1 h. To induce co-precipitation, an excess ammonia solution (~ 4 M) was added and the suspension was aged for 1 h under vigorous stirring. The co-precipitates were filtered, washed several times with deionized water, and finally dried overnight at 80 °C. Some GDC10 samples were prepared by adding 1 mol% Li_2O or CoO as sintering aids. Li_2O was added to GDC10 by impregnation in a concentrated solution of LiNO_3 ; the corresponding sample was labelled LiGDC10. For producing CoGDC10 composition, proper amount of $\text{Co}(\text{NO}_3)_2$ was dissolved into Ce and Gd nitrates solution before the co-precipitation. Hydrous cobalt oxide was formed together with the hydrous gadolinium-doped cerium oxide.

The synthesized powders were calcined at 400 °C for 1 h to promote the complete crystallization of the fluorite structure but limiting grain growth and agglomeration phenomena.

The thermal behavior of the samples was ascertained by simultaneous differential scanning calorimetry and thermogravimetric analysis (DSC and TGA, Thermoanalyzer STA 409, Netzsch) carried out in air up to 1200 °C using heating rate of 10 °C/min and $\alpha\text{-Al}_2\text{O}_3$ as a reference. The synthesized powder was also characterized by X-ray diffraction

(XRD) using a Panalytical X'PERT MPD diffractometer. To identify the cell parameter (a) and the primary particle size (D_{XRD}) of the samples, Rietveld refinement using MAUD suite [23] was carried out.

The specific surface area of the synthesized powders was obtained by nitrogen adsorption analysis (BET method) using a Micromeritics Gemini apparatus and using nitrogen as adsorbate gas; the sample was preliminarily dried under vacuum at 100 °C.

The calcined powders were compacted into cylindrical pellets by cold isostatic pressing at 160 MPa to be used for FS. The green specimens were inserted between two platinum disks ($\phi = 9$ mm, $h = 4$ mm) connected to a DC power supply (Sorensen DLM300). To ensure a good electrical contact with platinum disks, the flat surfaces of the specimens were painted with a silver-based conductive paste (Agar Scientific). A multimeter (Keithley 2100) recorded the applied voltage and the electrical current versus time.

The sample and the electrodes were placed in a dilatometer (Linseis L75) and heated at constant heating rate (20 °C/min). Once the sample reached 200 °C, the power supply was switched on, starting in this way the voltage control. In the present work, the electric field was applied in the range 25–250 V/cm. During FS phenomenon, the system switched from voltage to current control, being the current limit set at 13.5 mA/mm². After that, the current flowed for 2 min, and finally, the power supply and the furnace were switched off.

The apparent density of the sintered pellets was measured by using a hydrostatic balance (Archimedes' principle), and the microstructure was analyzed by SEM (Philips XL30) after careful polishing and thermal etching of the flat pellets surface.

Electrochemical impedance spectroscopy (EIS) measurements were taken on sintered pellets using symmetric electrodes. Both faces of the pellets were painted using gold conductive paste before a thermal treatment at 600 °C for 1 h to ensure good adhesion and proper electric contact. EIS measurements were taken in the 300–800 °C temperature range using a frequency response analyzer (FRA, Solartron 1260), coupled with a dielectric interface (Solartron 1296), in a frequency range between 0.1 Hz and 1 MHz with an AC voltage amplitude of 100 mV. Fitting of impedance plots was carried out by ZsimpWin software.

Results and discussion

Gd- and Sm-doped ceria co-precipitates

Figure 1 shows the XRD patterns of as-synthesized GDC10 and SDC10 powders, where the fluorite peaks are clearly detectable and their broadness indicates a nanometric crystallites size. These findings are in agreement with the results of Shih et al. [24] who reported that precipitated ceria begins to crystallize even at 0 °C. Moreover, the diffraction pattern shape suggests the presence of a certain amount of amorphous phase, as also previously reported [10, 18]. All co-precipitated samples showed similar XRD diffractograms. The nanometric size of the powders is confirmed by their specific surface area, which is 105 and 96 m²/g for GDC10 and SDC10, respectively. From such values, the particles average diameter can be estimated being equal to about 8 and 9 nm for GDC10 and SDC10, respectively. DSC-TG analysis confirms the presence of a certain amount of amorphous phase. The thermal behavior of as-synthesized SDC10 powder is reported in Fig. 2, and it is similar to that of other co-precipitated compounds [10, 18]. An exothermic peak at 284 °C can be associated with the crystallization of the amorphous phase, and the corresponding weight loss is ascribable to the decomposition of the amorphous hydrated compound to anhydrous crystalline oxide [10, 18].

As also reported in a previous work [18], after the crystallization of the amorphous phase, no additional phase transformation or formation of secondary phases occurred even at temperatures as high as 1000 °C, indicating that the solid solution of Gd or

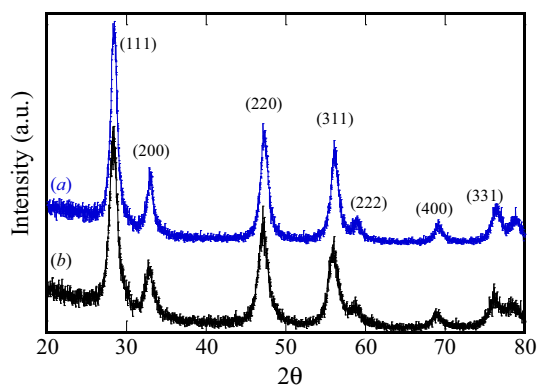


Figure 1 XRD pattern of as-synthesized GDC10 (a) and SDC10 (b) powders.

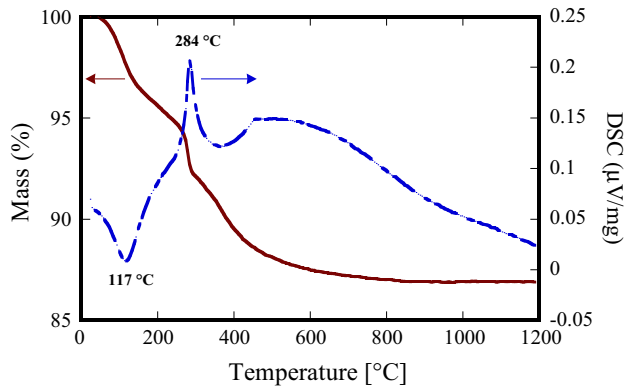


Figure 2 DSC (dashed line) and TG (solid line) of as-synthesized SDC10 powder.

Sm within the CeO₂ fluorite structure is stable over a wide temperature range.

The calcination at 400 °C for 1 h allows the complete formation of a single fluorite phase as shown by XRD patterns of GDC10 and SDC10 powders reported in Fig. 3. The cell parameter and the crystal size, calculated by using Rietveld refinement method, are reported in Table 1 for both as-synthesized and calcined GDC and SDC powders. As evident in this table, the mild calcination step preserves the nanometric size of the powders. The calculated cell

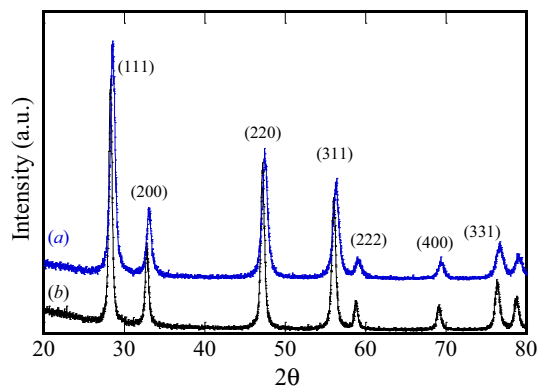


Figure 3 XRD pattern of GDC10 (a) and SDC10 (b) powders calcined at 400 °C for 1 h.

Table 1 Cell parameter and crystal size of synthesized and calcined powders

Sample	Cell parameter (nm)	Crystallite size (nm)
GDC10	$0.5432 \pm 3.7E-5$	10.8 ± 0.11
GDC10 calcined	$0.5418 \pm 1.7E-5$	20.1 ± 0.13
SDC10	$0.5447 \pm 5.3E-5$	9.3 ± 0.15
SDC10 calcined	$0.5440 \pm 2.6E-5$	26.8 ± 0.37

parameter is in good agreement with the literature data, being equal to 0.5418 nm (ICDD reference pattern n. 75-161) and 0.5423 nm (ICDD reference pattern n. 75-157) for GDC10 and SDC10, respectively.

Flash sintering

The FS phenomenon was observed in all tested samples. The onset temperature for FS, defined as the temperature at which the power supply switches from voltage to current control, is reported in Fig. 4 as a function of the electric field. In agreement with previous results [25], FS temperature decreases when a larger electrical field is applied. In any case, the flash sintering temperature is always well below the values typically required for conventional sintering.

The onset temperature is influenced by the presence of dopants and sintering aids. Specifically, a larger Gd or Sm doping accounts for lower FS temperatures being the reduction particularly significant up to 10 mol% doping (about 200 °C). The use of sintering aids such as Li₂O drastically reduces FS temperature by more than 100 °C, while CoO does not seem to significantly affect the behavior (<35 °C).

It is well known that the onset temperature for FS is related to the specific power dissipation (P) trend. Figure 5 shows how P changes with the furnace temperature for samples subjected to 100 V/cm. For all samples, a deviation from linearity occurs for $P \sim 15 \text{ mW/mm}^3$, in agreement with previous results [19, 22, 26–28]. The flash phenomenon is observed $\sim 30\text{--}60 \text{ s}$ (10–20 °C) after that the power dissipation value is reached. This behavior is very likely due to the fact that, once the threshold specific power is reached, the sample is no more able to dissipate the internal heat generated by Joule effect and it undergoes to a rapid and uncontrolled heating [25]. After that, the system switches from voltage to current control and the “flash event” occurs. One can also observe that, during the incubation, when the system is under voltage control, the specific power dissipation increases with Gd or Sm content up to 10 mol%, while further dopant additions do not lead to significant changes. Also Li addition drastically increases power dissipation during FS incubation, while no relevant effects can be observed in Co-containing material.

From comparison of Figs. 4 and 5, the onset temperature is lower for the specimens that showed a higher power dissipation during FS incubation.

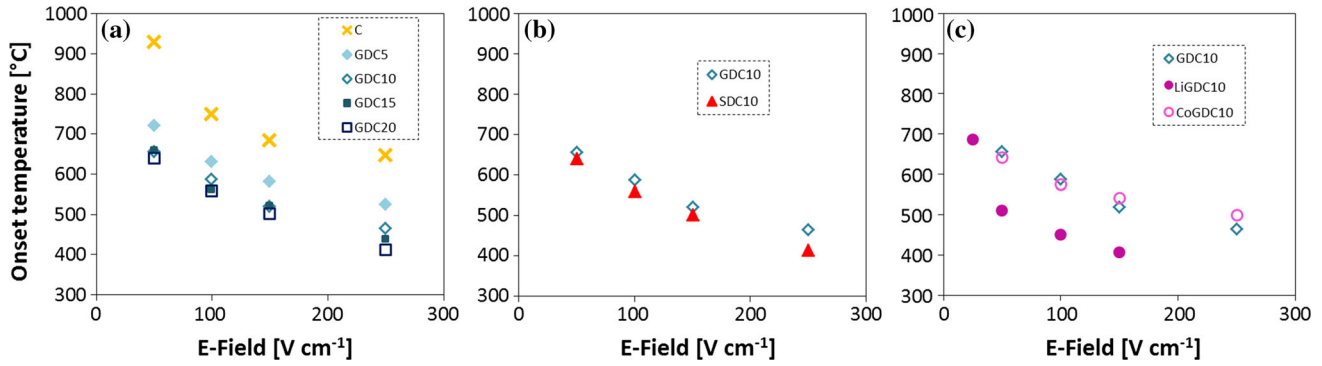


Figure 4 Onset temperature for FS as a function of the applied electrical field.

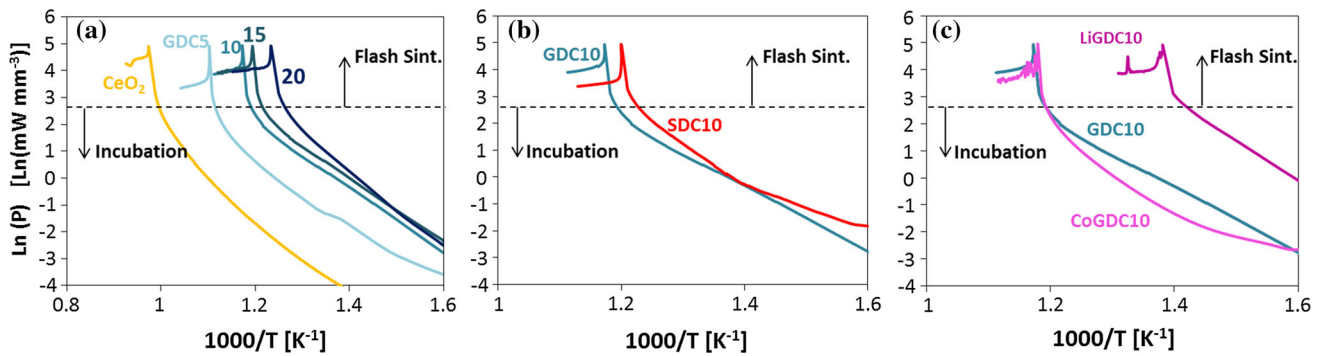


Figure 5 Specific power dissipation as a function of the furnace inverse temperature (for electrical field equal to 100 V/cm).

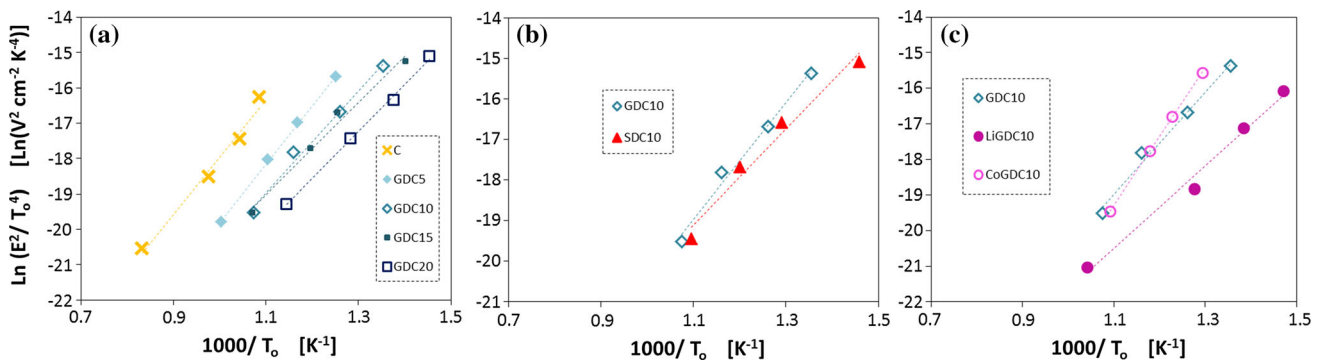


Figure 6 Relation between electric field (E) and onset flash sintering temperature (T_0) in the $\ln(E^2/T_0^4)$ versus $1000/T_0$ plots. The interpolation using Eq. (2) is represented by the *dashes lines*.

When the system is under voltage control (FS incubation stage), power dissipation linearly increases by increasing the green body conductivity; in other words, green pellets with larger conductivity are characterized by larger P values and lower onset temperature (for the same electric field). Therefore, controlling the type and the amount of dopant, it is possible to change the green body conductivity and decrease the onset sintering temperature further.

An analytical correlation between the onset temperature for FS (T_0) and the electrical parameters of the system was developed by Dong et al. [29, 30] and is reported in Eq. (2):

$$\ln\left(\frac{E^2}{T_0^4}\right) = \frac{E_a}{RT_0} + B \tag{2}$$

where E_a is the activation energy for conduction in the green body, R is the perfect gas constant and B is

Table 2 Activation energy for conduction as estimated from the power dissipation plot (Fig. 5) and from the onset flash sintering temperature (Fig. 6, Eq. (2))

Sample	E_a [eV]	
	Power plots	Onset temperature
CeO ₂	1.19 ± 0.25	1.40
GDC5	1.01 ± 0.10	1.42
GDC10	0.95 ± 0.09	1.24
GDC15	1.04 ± 0.07	1.12
GDC20	1.10 ± 0.08	1.15
SDC10	0.93 ± 0.15	1.02
LiGDC10	1.05 ± 0.21	1.00
CoGDC10	1.04 ± 0.17	1.65

a constant depending on the geometrical and radiative parameters of the system.

In Fig. 6, the parameters measured during the FS are reported. According to Eq. (2), a linear behavior ($R^2 \geq 0.976$) is obtained. The activation energy for conduction in the green specimen can be estimated from the slope of Fig. 6, and it can be compared to the activation energy measured from the power dissipation during the incubation of flash sintering (Fig. 5). E_a values estimated by the two methods are reported in Table 2. E_a ranges between 0.93 and 1.65 eV in good agreement with the activation energy measured in dense electrolytes [27, 31–34]. The activation energy values obtained by the two methods are pretty similar, supporting the validity of the developed model to evaluate the onset temperature for flash sintering.

Microstructure of the sintered samples

In the presence of Li as sintering aid, the FS temperature decrease plays a negative role on densification. The temperature at which the flash sintering occurs is probably too low and the sample cannot attain a satisfactory densification. The fracture surface at different magnifications of the sample flash-sintered at 100 V/cm is shown in Fig. 7a, b. A homogenous grain size of about 500 nm is clearly revealed. In Table 3, the grain size values of pellets sintered at 100 V/cm and calculated by Rietveld refinement are reported. The calculated value for LiGDC10 sample is in agreement with the microstructural investigation. A distributed nano-sized porosity is also revealed, and it causes a

Figure 7 SEM micrographs of samples flash-sintered under 100 V/cm: LiGDC10 (a, b), CoGDC10 (c, d), GDC10 (e, f), and SDC10 (g, h).

relatively low density of 67%, as reported in Table 4 showing the relative density values of flash-sintered samples. Moreover, the sample sintered at 50 V/cm has a relative density of 71%. This feature can be considered as a further confirmation of the fact that the reduced FS temperature is the main reason of the quite poor densification. Therefore, according to our results, the use of Li as sintering aid in FS of Gd-doped ceria ceramics appears not only useless, but even counterproductive. As shown in Fig. 7 and confirmed by the values reported in Table 4, the grain size of the other FS samples is definitely smaller and similarly for the pores size. Thus, it seems that coarsening rather than densification occurs during FS of LiGDC10 samples.

The other samples CoGDC10, GDC10, and SDC10 are quite similar from a microstructural point of view (Fig. 7). CoGDC10 and SDC10 are not completely homogeneous and are formed by nearly fully dense regions alternated to porous regions (Fig. 7c, g) although relatively high density is achieved especially for the former sample (Table 4). The microstructure of the dense regions in CoGDC10 and SDC10 is reported in Fig. 7d, h, respectively, where a very limited grain size is evident, further confirmed by the calculated grain size values reported in Table 3 (being 95 and 51 nm for CoGDC10 and SDC10, respectively). Conversely, GDC10 sample is properly densified (98–99% relative density) with a fine and homogeneous grain size of 200–300 nm, as reported in Fig. 7e, f. To justify the different behavior of SDC10 and GDC10 samples, it can be considered the crystal size before and after calcination. From data reported in Table 1, calcination is responsible for the growth of crystal size of about 85% and about 190% for GDC10 and SDC10, respectively. As reported by some authors of this paper [35], the ratio between crystal size after and before calcination can be used as a rough estimation of the agglomeration degree. Thus, SDC10 powders are much more agglomerated than the GDC10 ones and this fact can inhibit a full densification.

Finally, it is important to point out that no macroscopic inhomogeneity was present in the electrode areas. During DC flash sintering experiments,

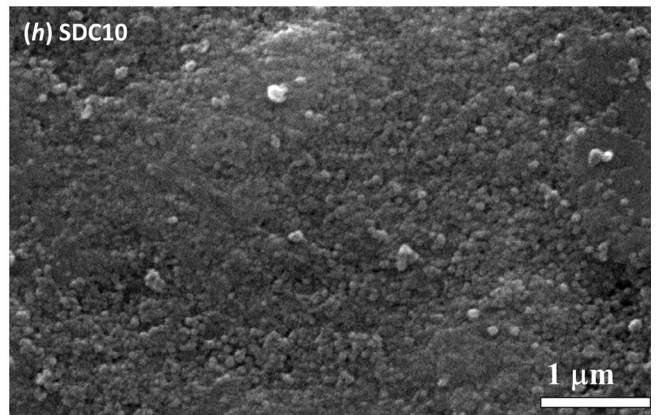
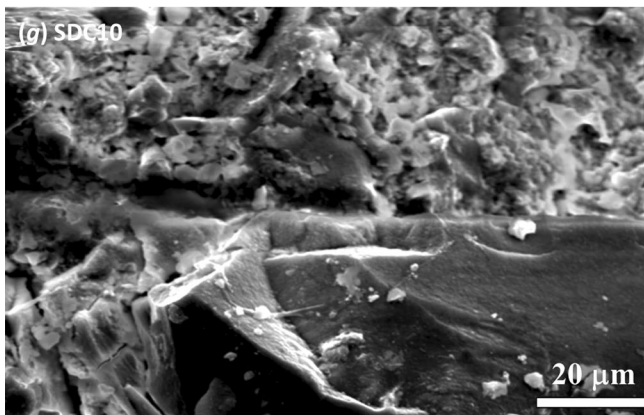
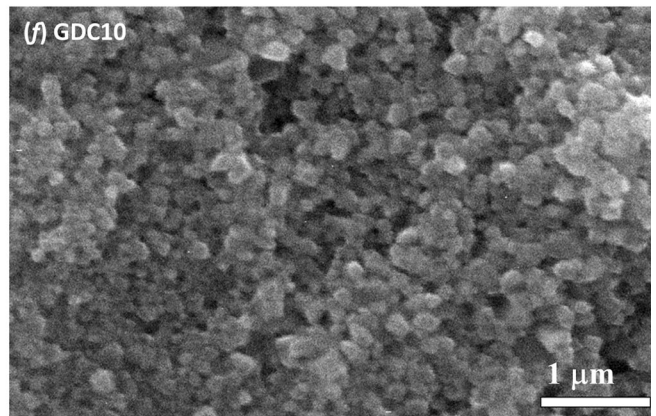
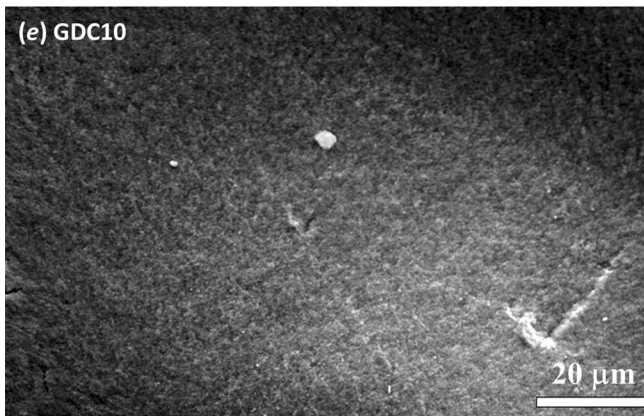
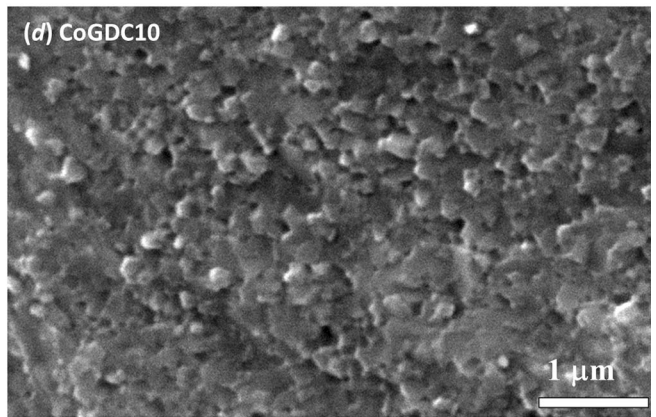
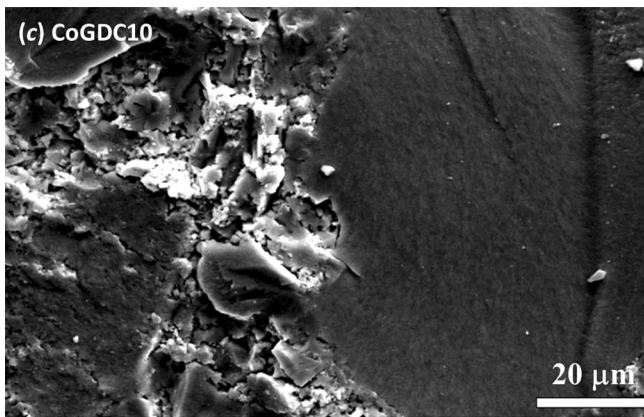
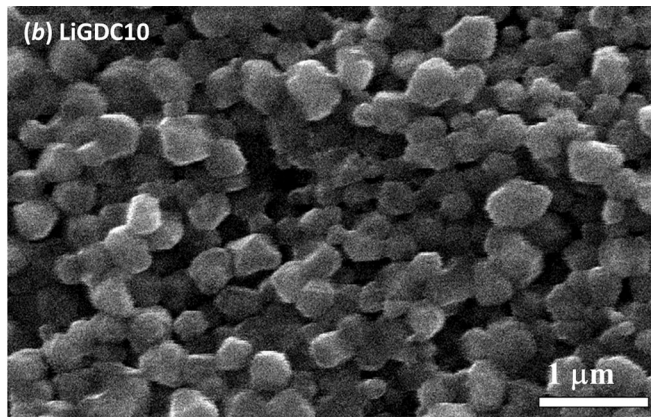
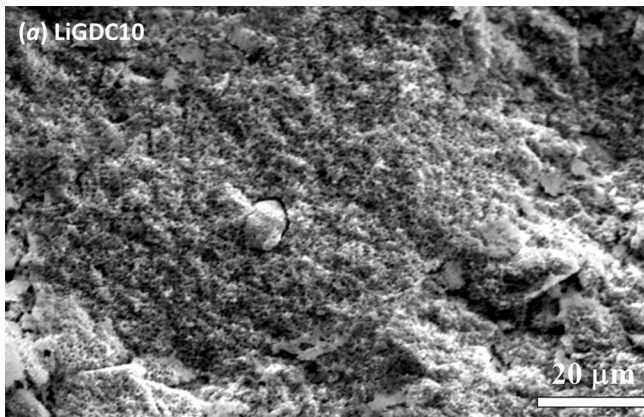


Table 3 Grain size of samples flash-sintered at 100 V/cm

Sample	Grain size (nm)
GDC10	208 ± 11
LiGDC10	410 ± 9.0
CoGDC10	95 ± 2.5
SDC10	51 ± 0.7

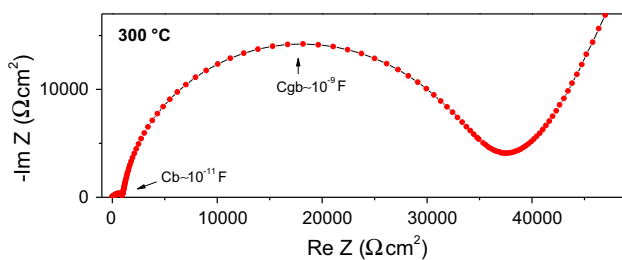
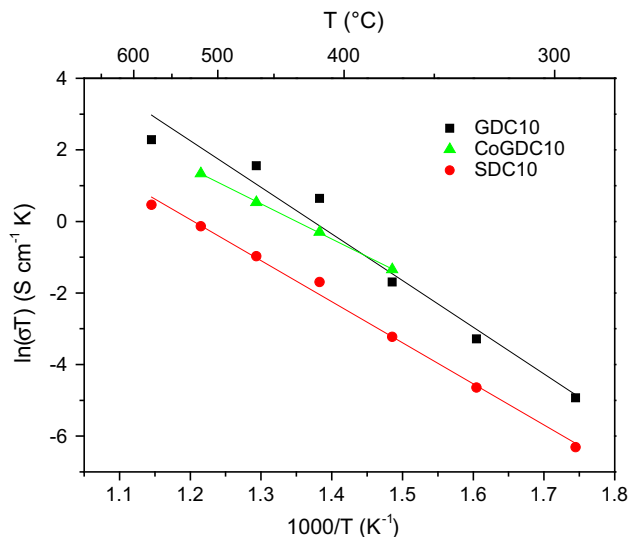
Table 4 Relative density (%) of flash-sintered samples

Sample	50 V/cm	100 V/cm
GDC10	97.9 ± 1.4	98.9 ± 0.2
LiGDC10	70.9 ± 1.3	67.0 ± 0.4
CoGDC10	93.2 ± 0.7	93.3 ± 0.7
SDC10	68.9 ± 0.4	75.2 ± 2.1

YSZ was previously shown to be partially reduced, producing “blackened zones”; such areas are generally concentrated in the cathodic region and they can be easily observed by naked eye [36]. These are not visible on the samples prepared in the present work. This can be very likely associated with the fact that the used current limit (13.5 mA/mm²) is lower than that typically used for YSZ flash sintering experiments [37]; therefore, reduction phenomena are more unlikely to occur. Moreover, no second phase associated with ceria reduction (i.e., Ce₂O₃) can be detected from XRD patterns. However, this is not excluding that some Ce⁴⁺ can be reduced to Ce³⁺ during the process, forming a dilute solid solution.

Electrical characterization

The electrical behavior of sintered samples was measured in the temperature range between 300 and 600 °C in synthetic air. As an example, Fig. 8 shows the Nyquist plots for GDC10 at 300 °C, revealing two separated semicircles associated with bulk and grain boundary contribution at low temperature;

**Figure 8** Nyquist plot of GDC10 at 300 °C.**Figure 9** Arrhenius plot of GDC10, CoGDC10, and SDC10 samples flash-sintered under 100 V/cm.

conversely, only one semicircle was measured at high temperature. The same behavior was recorded also on the other materials. The total resistivity was calculated by using a $(R - CPE)_b(R - CPE)_{gb}(R - CPE)_{el}$ equivalent circuit at low temperature and a $R_t(R - CPE)_{el}$ equivalent circuit at high temperature, being R_t the total resistivity. In the former case, the main contribution to the total resistivity is due to the low frequency arc associated with a capacity of 10^{-9} F and, therefore, correlated with the grain boundary contribution. The large grain boundary resistance revealed at low temperature for GDC10 is in agreement with the nanometric morphology reported in Fig. 7e, f.

Figure 9 shows the Arrhenius plot of the ionic conductivity of GDC10, CoGDC10, SDC10 flash-sintered under electric field of 100 V/cm. GDC10 sample shows the highest conductivity equal to 1.13×10^{-2} S/cm at 600 °C with an activation energy E_a equal to 1.1 eV. Such values are comparable to the literature data for GDC10 conventionally sintered at 1500 °C [28, 31–34]. CoGDC10 sample, having a relative density of 93%, shows slightly lower conductivity. Conversely, conductivity decreases significantly in SDC10 sample, this being related to the lower density.

For all samples (except LiGDC10), a reduction in the electric field intensity (from 100 to 50 V) accounts for lower conductivity, as it is expected from microstructural features.

Conclusions

Nanocrystalline Gd- and Sm-doped ceria powders synthesized by co-precipitation method were successfully consolidated by flash sintering procedure at temperatures between 600 and 900 °C under an electric field ranging from 5 to 250 V/cm. Quite surprisingly, the addition of Li₂O and CoO as sintering aids does not improve the densification. Fully dense (99%) GDC10 samples with grain size of about 200–300 nm can be flash-sintered at temperatures slightly lower than 600 °C. The total conductivity at 600 °C was 1.13×10^{-2} S/cm a value comparable to that measured on samples conventionally sintered at 1500 °C. Conversely, SDC10 samples processed using the same conditions maintain a certain amount of porosity, which is responsible for lower conductivity values.

Acknowledgements

The financial support and collaboration of INSTM and Fondazione Caritro (Cassa di Risparmio di Trento e Rovereto) (Project 2015: Sviluppo di SOFC planari operanti a temperature intermedie con combustibili derivanti da biomasse (biogas) (BioplanarSOFC) are gratefully acknowledged.

Compliance with ethical standards

Conflict of interest The authors declare that they have no conflict of interest.

References

- [1] Wang SF, Yeh CT, Wang YR, Wu YC (2013) Characterization of samarium-doped ceria powders prepared by hydrothermal synthesis for use in solid state oxide fuel cells. *J Mater Res Technol* 2:141–148. doi:10.1016/j.jmrt.2013.01.004
- [2] Stojmenovic M, Boskovic S, Zunic M, Babic B, Matovic B, Bajuk-Bogdanovic D, Mentus S (2015) Studies on structural, morphological and electrical properties of Ce_{1-x}Er_xO_{2-δ} ($x = 0.05-0.20$) as solid electrolyte for IT-SOFC. *Mater Chem Phys* 153:422–431. doi:10.1016/j.matchemphys.2015.01.036
- [3] Rambabu B, Ghosh S, Jena H (2006) Novel wet-chemical synthesis and characterization of nanocrystalline CeO₂ and Ce_{0.8}Gd_{0.2}O_{1.9} as solid electrolyte for intermediate temperature solid oxide fuel cell (IT-SOFC) applications. *J Mater Sci* 41:7530. doi:10.1007/s10853-006-0837-6
- [4] Singh V, Babu S, Kakakoti AS, Agarwal A, Seal S (2010) Effect of submicron grains on ionic conductivity of nanocrystalline doped ceria. *J Nanosci Nanotechnol* 10: 6495–6503. doi:10.1166/jnn.2010.2523
- [5] Esposito V, Traversa E (2008) Design of electroceramics for solid oxides fuel cell applications: playing with ceria. *J Am Ceram Soc* 91:1037–1051. doi:10.1111/j.1551-2916.2008.02347.x
- [6] Donmez G, Sariboga V, Altincekic TG, Oksuzomer MAF (2015) Polyol synthesis and investigation of Ce_{1-x}RE_xO_{2-x/2} (RE = Sm, Gd, Nd, La, $0 \leq x \leq 0.25$) electrolytes for IT-SOFCs. *J Am Ceram Soc* 98:501–509. doi:10.1111/jace.13300
- [7] Kuharuangrong S (2007) Ionic conductivity of Sm, Gd, Dy and Er-doped ceria. *J Power Source* 171:506–510. doi:10.1016/j.jpowsour.2007.05.104
- [8] Balazs GB, Glass RS (1995) AC impedance studies of rare earth oxide doped ceria. *Solid State Ionics* 76:155–162. doi:10.1016/0167-2738(94)00242-K
- [9] Shannon RD (1976) Revised effective ionic radii and systematic studies of interatomic distances in halides and chalcogenides. *Acta Cryst A* 32:751–767. doi:10.1107/S0567739476001551
- [10] Dell'Agli G, Spiridigliozzi L, Marocco A, Accardo G, Ferone C, Cioffi R (2016) Effect of the mineralizer solution in the hydrothermal synthesis of Gadolinium-doped (10% molGd) ceria nanopowders. *J Appl Biomater Funct Mater* 14:e189–e196. doi:10.5301/jabfm.5000282
- [11] Accardo G, Ferone C, Cioffi R, Frattini D, Spiridigliozzi L, Dell'Agli G (2016) Electrical and microstructural characterization of ceramic gadolinium-doped ceria electrolytes for ITSOFCs by sol–gel route. *J Appl Biomater Funct Mater* 14:e35–e41. doi:10.5301/jabfm.5000265
- [12] Accardo G, Spiridigliozzi L, Cioffi R, Ferone C, Di Bartolomeo E, Yoon SP, Dell'Agli G (2017) Gadolinium-doped ceria nanopowders synthesized by urea-based homogeneous co-precipitation (UBHP). *Mat Chem Phys* 187:149–155. doi:10.1016/j.matchemphys.2016.11.060
- [13] Spiridigliozzi L, Dell'Agli G, Biesuz M, Sglavo VM, Pansini M (2016) Effect of the precipitating agent on the synthesis and sintering behaviour of 20 mol% Sm-doped ceria. *Adv Mater Sci Eng* 2016:8. doi:10.1155/2016/6096123 [Article ID 6096123]
- [14] Kleinlogel C, Gaukler LJ (2000) Sintering and properties of nanosized ceria solid solutions. *Solid State Ionics* 135:567–573. doi:10.1016/S0167-2738(00)00437-9
- [15] Van Herle J, Horita T, Kawada T, Sakai N, Yokohama H, Dokiya M (1997) Fabrication and sintering of fine yttria-

- doped ceria powder. *J Am Ceram Soc* 80:933–940. doi:10.1111/j.1151-2916.1997.tb02924.x
- [16] Dong Y, Wang H, Chen I-W (2017) Electrical and hydrogen reduction enhances kinetics in doped zirconia and ceria: I. Grain growth study. *J Am Ceram Soc*. doi:10.1111/jace.14615
- [17] Inaba H, Nakajima T, Takawa H (1998) Sintering behaviors of ceria and gadolinia-doped ceria. *Solid State Ionics* 106:263–268. doi:10.1016/S0167-2738(97)00496-7
- [18] Biesuz M, Dell’Agli G, Spiridigliozzi L, Ferone C, Sglavo VM (2016) Conventional and field-assisted sintering of nanosized Gd-doped ceria synthesized by co-precipitation. *Ceram Int* 42:11766–11771. doi:10.1016/j.ceramint.2016.04.097
- [19] Downs JA, Sglavo VM (2013) Electric field assisted sintering of cubic zirconia at 390 °C. *J Am Ceram Soc* 96:1342–1344. doi:10.1111/jace.12281
- [20] Cologna M, Rashkova B, Raj R (2010) Flash sintering of nanograin zirconia in <5 s at 850 °C. *J Am Ceram Soc* 93:3556–3559. doi:10.1111/j.1551-2916.2010.04089.x
- [21] Muccillo R, Kleitz M, Muccillo ENS (2011) Flash grain welding in yttria stabilized zirconia. *J Eur Ceram Soc* 31:1517–1521. doi:10.1016/j.jeurceramsoc.2011.02.030
- [22] Hao X, Liu Y, Wang Z, Qiao J, Sun K (2012) A novel sintering method to obtain fully dense gadolinia doped ceria by applying a direct current. *J Power Sour* 210:86–91. doi:10.1016/j.jpowsour.2012.03.006
- [23] Lutterotti L, Bortolotti M, Ischia G, Lonardelli I, Wenk HR (2007) Rietveld texture analysis from diffraction images. *Z Fur Krist Suppl* 1:125–130. doi:10.1524/zksu.2007.2007.suppl_26.125
- [24] Shih CJ, Chen YJ, Hon MH (2010) Synthesis and crystal kinetics of cerium oxide nanocrystallites prepared by co-precipitation process. *Mater Chem Phys* 121:99–102. doi:10.1016/j.matchemphys.2010.01.001
- [25] Todd RI, Zapata-Solvas E, Bonilla RS, Sneddon T, Wilshaw PR (2015) Electrical characteristics of flash sintering: thermal runaway of joule heating. *J Eur Ceram Soc* 35:1865–1877. doi:10.1016/j.jeurceramsoc.2014.12.022
- [26] Biesuz M, Sglavo VM (2016) Flash sintering of alumina: effect of different operating conditions on densification. *J Eur Ceram Soc* 36:2535–2542. doi:10.1016/j.jeurceramsoc.2016.03.021
- [27] Biesuz M, Sglavo VM (2017) Liquid phase flash sintering in magnesia silicate glass-containing alumina. *J Eur Ceram Soc* 37(2):705–713. doi:10.1016/j.jeurceramsoc.2016.08.036
- [28] Biesuz M, Luchi P, Quaranta A, Sglavo VM (2016) Theoretical and phenomenological analogies between flash sintering and dielectric breakdown in α -alumina. *J Appl Phys* 120:145107. doi:10.1063/1.4964811
- [29] Dong Y, Chen I-W (2015) Predicting the onset of flash sintering. *J Am Ceram Soc* 98:2333–2335. doi:10.1111/jace.13679
- [30] Dong Y, Chen I-W (2015) Onset criterion for flash sintering. *J Am Ceram Soc* 98:3624–3627. doi:10.1111/jace.13866
- [31] Ramos-Alvarez P, Villafuerte-Castrejon ME, Gonzalez G, Cassir M, Flores-Morales C, Chavez-Carvayar JA (2016) Ceria-based electrolytes with high surface area and improved conductivity for intermediate temperature solid oxide fuel cells. *J Mater Sci* 52:519–532. doi:10.1007/s10853-016-0350-5
- [32] Inaba H, Tagawa H (1996) Ceria-based solid electrolytes. *Solid State Ionics* 83:1–16. doi:10.1016/0167-2738(95)00229-4
- [33] Lewis GS, Atkinson A, Steele BCH, Drennan J (2002) Effect of Co addition on the lattice parameter, electrical conductivity and sintering of gadolinia-doped ceria. *Solid State Ionics* 152–153:567–573. doi:10.1016/S0167-2738(02)00372-7
- [34] Mogensen M, Sammes NM, Tompsett GA (2000) Physical, chemical and electrochemical properties of pure and doped ceria. *Solid State Ionics* 129:63–94. doi:10.1016/S0167-2738(99)00318-5
- [35] Dell’Agli G, Mascolo G (2001) Agglomeration of 3 mol% Y-TZP powders synthesized by hydrothermal treatment. *J Eur Ceram Soc* 21:29–35. doi:10.1016/S0955-2219(00)00171-0
- [36] Downs J (2013) Mechanisms of flash sintering in cubic zirconia. Ph.D. Thesis, University of Trento, <http://eprints-phd.biblio.unitn.it/976/>
- [37] Baraki R, Schwarz S, Guillon O (2012) Effect of electrical field/current on sintering of fully stabilized zirconia. *J Am Ceram Soc* 95:75–78. doi:10.1111/j.1551-2916.2011.04980.x